Chem. Res. Chin. Univ., 2018, 34(4), 684—690 doi: 10.1007/s40242-018-7413-x

Preparation and Properties of Magnetic-fluorescent Microporous Polymer Microspheres

ZOU Xiaohu, WEI Zhizhi, DU Jing, WANG Xiaotao and ZHANG Gaowen*

Hubei Provincial Key Laboratory of Green Materials for Light Industry, School of Materials and Chemical Engineering, Hubei University of Technology, Wuhan 430068, P. R. China

Abstract Microporous microspheres can be used as functional nanomaterial carriers for their microporous structure and higher specific surface area. In this study, magnetic fluorescent polymer microspheres were prepared by incorporating Fe_3O_4 nanoparticles and CdSe/ZnS quantum dots(QDs) into hyper-crosslinked microporous polymer microspheres(HCMPs) *via* the *in situ* coprecipitation method and swelling-diffusion. The HCMPs predominantly have micropores, and their specific surface area is as high as 703.4 m^2/g. The magnetic-fluorescent microspheres maintain the superparamagnetic behavior of Fe_3O_4, and the saturation magnetization reaches 38.6 A m^2/kg. Moreover, the composite microspheres exhibit an intense emission peak at 530 nm and achieve good fluorescence.

Keywords Microporous polymer; Magnetic-fluorescent polymer microsphere; Hyper-crosslinking; Superparamagnetism; Quantum dot

1 Introduction

Microporous organic polymers(MPOs)[1,2], including covalent organic frameworks(COFs)[3,4], polymers of intrinsic microporosity(PIMs)[5], conjugated microporous polymers (CMPs)[6] and hyper-crosslinked porous polymers(HCPs)[7,8], exhibit large specific surface areas, high che- mical stabilities and low skeleton density, which extend a wide range of applications in gas storage and separation[9—11], adsorption[12,13], catalysis[14], etc. However, most MOPs exhibit irregular structures. Recently, more attention has been paid to controlling the micro-morphology of MOPs and developing their applications[15—18]. Hyper-crosslinked microporous polymer microspheres(HCMPs) have been prepared by hyper-crosslinking, with microspheres having a certain degree of crosslinking serving as precursors. This has realized the control of the pore size and the functionalization of the pore surface on the premise of keeping regular spherical structures. HCMPs are considered promising carriers to produce magnetic-fluorescent microspheres with good properties for biomedical applications, broadening the scope of MOPs.

Magnetic fluorescence microspheres have both superparamagnetic and fluorescent properties, which make their performance and application range better than those of traditional single functional nanoparticles. Based on these properties, the multifunctional microspheres have wide applications in biomedical, bioengineering and cytology[19—22]. At present, the main preparation methods of magnetic fluorescent polymer microspheres include layer-by-layer self-assembly[23], polymerization[24], polymer embedding[25], and swelling method[26], etc. However, there are still many aspects that need to be further enhanced, such as simplifying experimental operations and improving the stability and capacity of magnetic and fluorescent materials. Xie *et al*.[27] synthesized magnetic fluorescent composite microspheres by using the electrostatic self-assembly method to control the number of magnetic particles and quantum dots layers to assemble. However, their synthetic process is quite tedious. Tu *et al*.[28] copolymerized the modified magnetic and fluorescent particles with polyfunctional microspheres; thus, the nanoparticles can be fixed inside the microspheres by chemical bonds. However, this process also has drawbacks in that the nanoparticles are easily agglomerated and unstable in the system. Using HCMPs as a carrier, it would be easy to realize a large loading of various kinds of functional substances, such as magnetic, fluorescent and bioactive substances.

In this report, we adopted a new strategy, in which magnetic fluorescent bifunctional microspheres were prepared by combining microporous microspheres with magnetic fluorescent materials. First, hyper-crosslinked microporous polymer microspheres(HCMPs) with high specific surface area and rich micropores were prepared based on a hypercrosslinking procedure. Then, *via* the rich pore structures, ferriferous oxide and CdSe/ZnS quantum dots(QDs) were loaded into the microporous polymer microspheres by *in situ* co-precipitation method and solvent swelling method, respectively. Through this pore structure, both the loading capacity and the stability of nanoparticles are improved. However, there are still some limitations in the research regarding HCMPs. At present, most of the polymer networks don't have regular structures, and few studies have been reported on the preparation of HCMPs with a spherical morphology. To solve this problem, reflux

*Corresponding author. Email: zhgw2003@hbut.edu.cn

Received December 18, 2017; accepted April 9, 2018.

Supported by the National Natural Science Foundation of China(Nos.11174075, 31303049).

precipitation polymerization was chosen to prepare microspheres with a high cross-linking degree. Then, with an external cross-linker, microporous polymer microspheres with a complete spherical morphology were synthesized *via* the Friedel-Crafts reaction, which laid a good foundation for loading the magnetic fluorescent nanoparticles.

2 Experimental

2.1 Materials

Styrene(St), acrylic acid(AA), acetonitrile, toluene, 1,2-dichloroethane(DCE), anhydrous ferric chloride($FeCl_3$), methanol, ethanol, ferric chloride hexahydrate($FeCl_3$ $6H_2O$), ferrous sulfate heptahydrate($FeSO_4$ $7H_2O$), and ammonia hydroxide(NH_3 H_2O) were analytical grade and purchased from the National Medicines Corporation Ltd. of China. Divinylbenzene(DVB, 45%, mass fraction), azodiisobutyronitrile (AIBN) and formaldehyde dimethyl acetal(FDA, 98%, mass fraction) were purchased from Aldrich. CdSe/ZnS quantum dots dispersed in *n*-hexane and stabilized with trioctylphosphine oxide were purchased from Wuhan Jiayuan Quantum Dots Technology Development Corporation(China).

2.2 Synthesis of Hyper-crosslinked Microporous Polymer Microspheres

The preparation route of hyper-crosslinked microporous polymer microspheres(HCMPs) is shown in Scheme 1.

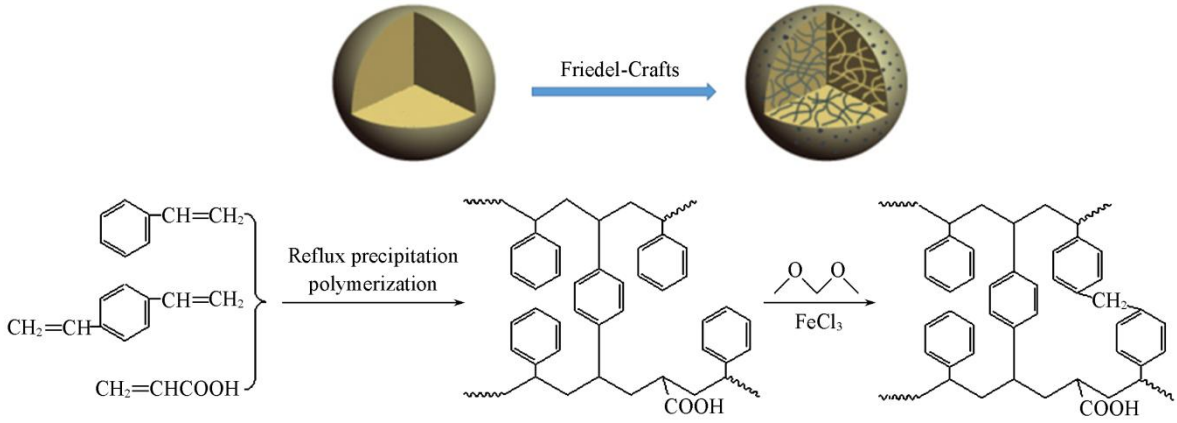

Scheme 1 Synthetic route of hyper-crosslinked microporous polymer microspheres

Polymerization of monodisperse crosslinked carboxyl-functionalized polystyrene-divinylbenzene-acrylic microspheres: St(0.5 mL), DVB(1.5 mL), AA(0.5 mL), and AIBN initiator(0.035 g) were heated in the mixed solution of acetonitrile(40 mL) and toluene(10 mL) at 84 °C for 2 h with magnetic stirring(600 r/min) in a round-bottomed flask with a reflux condenser. The formed microspheres were washed by extensive centrifugation cycles with methanol and finally dried by lyophilization.

Polymerization of hyper-crosslinked microporous polymer microspheres(HCMPs) was performed as follows: 3 g of dried P(St-DVB-AA) microspheres were swelled in DCE(60 mL) for 1 h under magnetic stirring(660 r/min) at 35 °C. Then, FDA(5.19 mL) and $FeCl_3$(9.33 g) were added to the swollen mixture. The original network was formed by stirring the mixture at 45 °C for 5 h *via* a Friedel-Crafts-type hyper-crosslinking reaction. Then, the mixture was heated at 80 °C for 19 h to obtain the porous polymer microspheres. After the reaction, the particles were separated and washed several times with methanol. The particles then were dried by lyophilization.

2.3 Synthesis of Magnetic Microporous Polymer Microspheres

A schematic illustration of the preparation of magnetic microspheres is shown in Scheme 2.

Magnetic microporous polymer microspheres were prepared by an *in situ* co-precipitation method. HCMPs(0.5 g) were dispersed in deionized water(100 mL) followed by the addition of $FeCl_3$ $6H_2O$(8.115 g) and $FeSO_4$ $7H_2O$(5.560 g) at

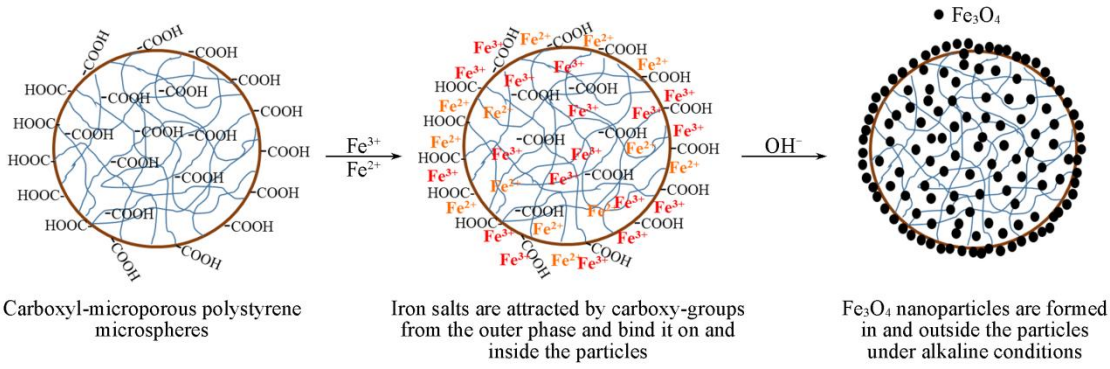

Scheme 2 Schematic illustration of preparation of magnetic microspheres by *in situ* co-precipitation method

a molar ratio of 3:2. The mixed solution was stirred under nitrogen for 1 h. After standing for 24 h, the solution was washed by extensive centrifugation cycles with ethanol and then placed in an alcohol-water solution. After that, ammonium hydroxide was slowly added to the mixture at 50 °C by using an injection pump until the pH value reached 9. The suspension was kept at 50 °C for 1 h, then washed with deionized water and ethanol several times and finally dried in a vacuum.

2.4 Synthesis of Magnetic-fluorescent Microporous Polymer Microspheres

A schematic illustration of the preparation of fluorescent microspheres is shown in Scheme 3.

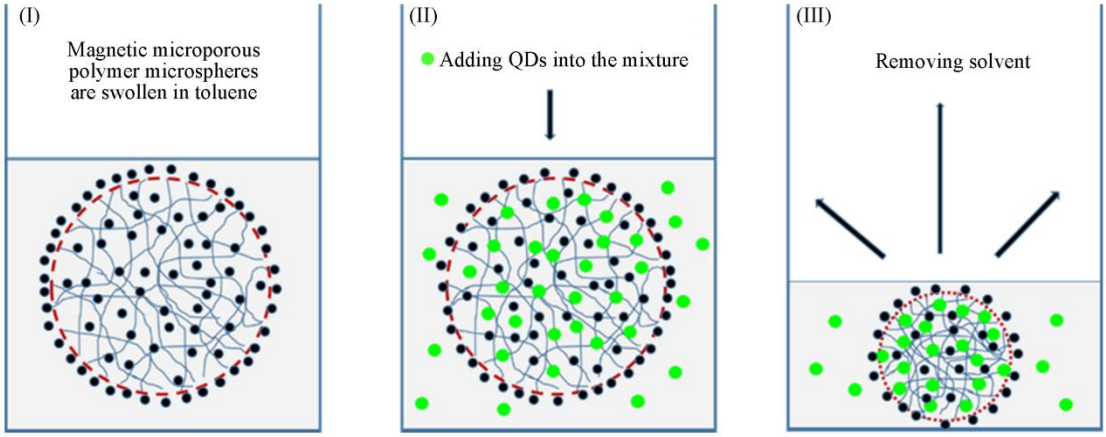

Scheme 3 Schematic illustration of preparation of magnetic-fluorescent microspheres by the swelling method

Fluorescent microporous polymer microspheres were prepared by the swelling method. The magnetic microspheres (30 mg) were swollen in toluene(5 mL) for approximately 1 h, followed by the addition of CdSe/ZnS quantum dots(40 μL, 16 μmol/L). The mixed solution was sonicated for 1 h, then placed into a Multitron shaker for 24 h. The resultant product was centrifuged and exhaustively washed with toluene several times and stored in toluene for later characterization.

2.5 Characterization

Fourier transform infrared spectroscopy(FTIR) was performed on a Tensor 2 spectrometer(Bruker Ltd., USA) at room temperature. Scanning electron microscopy(SEM) observation was carried out on a Hitachi S-4800 microscope(Hitachi Ltd., Japan) and a JSM-6390 microscope(JEOL Ltd., Japan). Polymer surface areas, N_2 adsorption isotherm(77 K) and pore size distributions were obtained with a Micromeritics ASAP 2020 surface area and porosimetry analyzer. The magnetic properties of the microspheres were measured by a PPMS-9T vibrating sample magnetometry(VSM) system(Quantum Design Ltd., USA). The photoluminescent measurements were carried out on an IX51 fluorescence spectrophotometer(Olympus, Japan). The excitation and emission spectra of the fluorescent HCMPs were acquired on the Cary Eclipse spectrometer(Varian, USA).

3 Results and Discussion

3.1 Infrared Spectra Analysis

Fig.1 shows the FTIR spectrum of polymer microspheres before being hyper-crosslinked(Fig.1 curve *a*) and after being hyper-crosslinked(Fig.1 curve *b*). The two curves both show a broad band at 3448 cm^{-1} corresponding to the O—H stretching vibration, a band at 1712 cm^{-1} corresponding to the C═O stretching vibration and a band at 1167 cm^{-1} corresponding to the C—O stretching vibration. The band at 3020 cm^{-1} belongs to the C—H stretching vibration of benzene, and the peaks at 1607, 1500 and 1445 cm^{-1} are attributed to the benzene ring skeleton vibrations. The band of the disubstituted benzene ring in the *para* position is at 833 cm^{-1}. The absorptions at 2925 and 2858 cm^{-1} originate from —CH_2— stretching vibrations. The results of FTIR confirm the copolymerization of styrene, divinylbenzene and acrylic acid. Comparing Fig.1 curves *a* and *b*, the positions of the absorption peaks are substantially the same but varies in the intensity of the peaks. After the hyper-crosslinking procedure, the adsorptions of the disubstituted benzene ring at the *para* position and the —CH_2— stretching vibrations are obviously enhanced as a result of the formation of methylene bridge between the benzene rings in the Friedel-Crafts reaction.

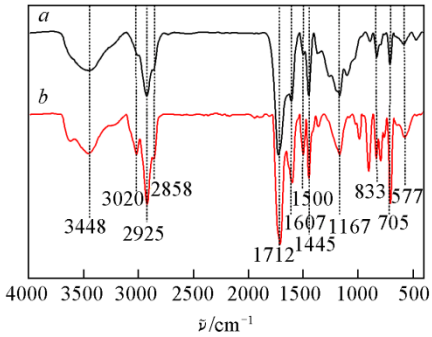

Fig.1 FTIR spectra of polymer microspheres before(*a*) and after hyper-crosslinking(*b*)

3.2 Morphology of HCMPs

The morphologies of microspheres before and after the hyper-crosslinking reaction are shown in Fig.2. Before hyper-crosslinking, the P(St-DVB-AA) precursors present a smooth surface with no obvious porous structure. After the

hyper-crosslinking reaction, the microporous microspheres present an obviously coarse surface with visible pores. The presence of dark and white contrast on the surface is ascribed to the existence of extensive micropores. This result proves that the polymer microspheres form rich pore structures during the hyper-crosslinking reaction.

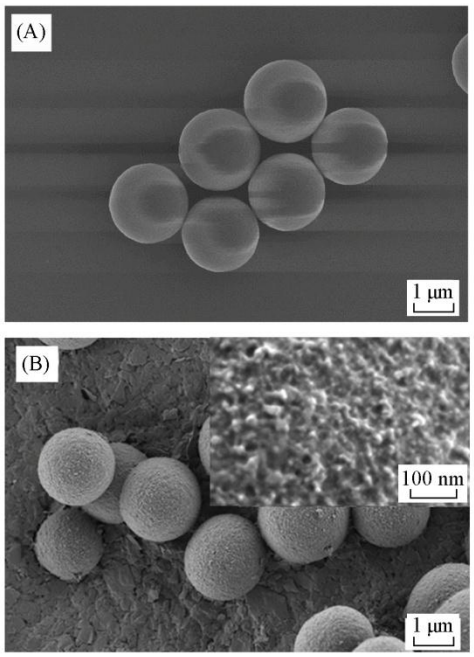

Fig.2 FE-SEM images of microspheres before(A) and after(B) the hyper-crosslinking reaction
Inset of (B): local magnification of microsphere surface.

3.3 Surface Area and Pore Size Distribution

Surface area and pore size distribution were characterized by nitrogen sorption analysis measured at 77 K. The BET surface area values of the highly crosslinked HCMPs are relatively high compared to that of HCMPs with a lower crosslinking degree(Table 1). The HCMPs with 80% DVB have the highest surface area, up to 703.4 m^2/g. The nitrogen adsorption-desorption isotherms at 77 K(Fig.3) and the pore size distribution analysis of HCMPs with various DVB contents(mass fraction) calculated by DFT methods(Fig.4) correspond to each other. As shown in Fig.3, all the polymer networks show Type-I nitrogen sorption isotherms according to the IUPAC classification and show a rapid uptake at low pressure(p/p_0<0.001), indicating a permanent microporous nature. A sharp rise in the nitrogen adsorption isotherms can be observed at medium and high relative pressures when the DVB content is 20% (p/p_0=0.42—1.0), which indicates the presence of some mesopores in the polymer networks. These results are probably due to inter-particle aggregation or voids[29]. Significant hysteresis loops can be observed in the medium and high-pressure region (p/p_0=0.42—1.0) when the DVB contents are 40%, 60% and 80%, which indicates the presence of mesopores in the materials. At the high pressure region(p/p_0>0.9), no steep rise in nitrogen adsorption occurs, indicating that there no macroporous structure existed in the networks. The results indicate that the pore diameter decreases with an increase of the degree of cross-linking, causing the pores of the microspheres to change from mesopores to micropores.

Table 1 Specific surface area of HCPMs

No.	DVB content (mass fraction, %)	Particle size/μm	S_{BET}*/(m^2 g^{-1})
1	20	1.91	4.4
2	40	2.18	281.8
3	60	2.26	610.1
4	80	4.36	703.4

* Surface area calculated from nitrogen adsorption isotherms at 77 K using the BET equation.

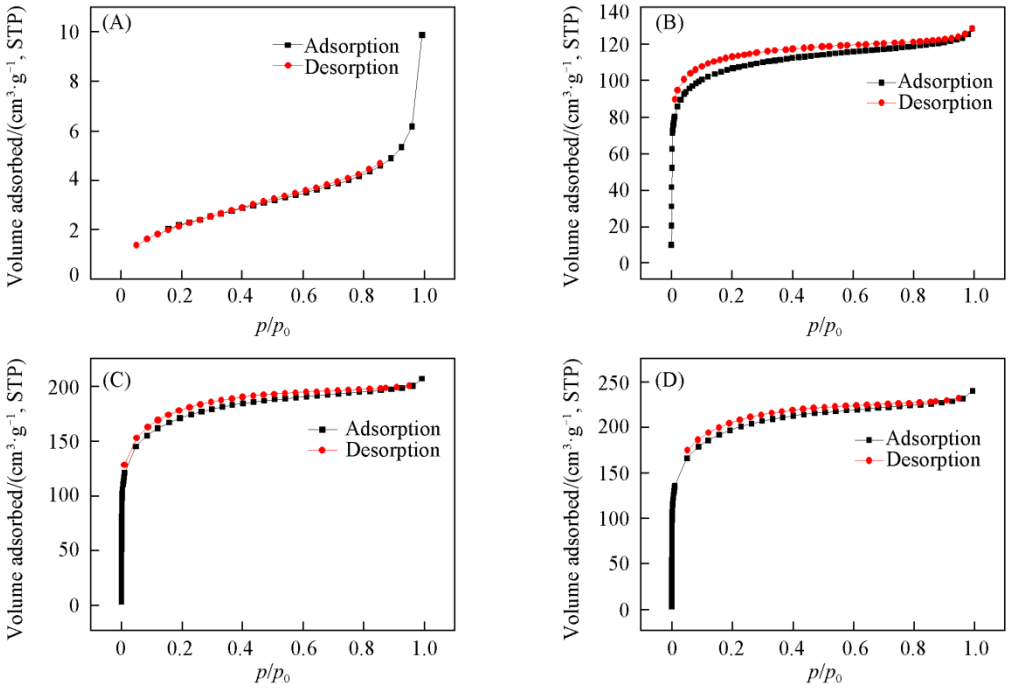

Fig.3 Nitrogen sorption isotherms of HCMPs with different concentrations of DVB at 77 K
Mass fraction of DVB(%): (A) 20; (B) 40; (C) 60; (D) 80.

The pore size distribution of the polymer was calculated from the adsorption branch of the isotherms with the DFT method. As shown in Fig.4, the micropore size range is mainly between 7—20 nm when the DVB content is 20%. When the DVB contents are 40%, 60% and 80%, the pore size distribution is in the range of 0.7—3 nm.

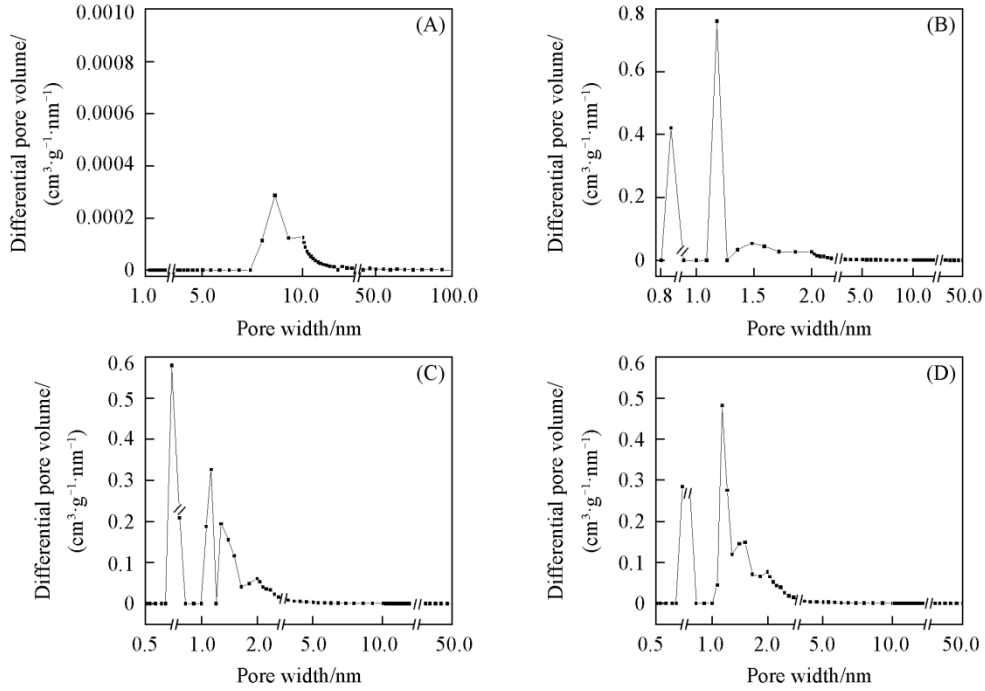

Fig.4 Pore size distributions of HCMPs with different concentrations of DVB calculated using DFT methods(slit pore, N_2-DFT models) at 77 K

Mass fraction of DVB(%): (A) 20; (B) 40; (C) 60; (D) 80.

Fig.5 shows the *T*-plot obtained from nitrogen adsorption at 77 K. At low pressure, adsorption first occurs in the micropores. Once the micropores are filled, adsorption only takes place on the external surface of the micropores. The *T*-plot provides an estimate of the external surface area and microporous volume of the particles. The classical way to determine the microporous volume of a material by the *T*-plot method is to extrapolate the linear fit in the low-pressure range and to take the intercept as the microporous volume[30]. As shown in Fig.5, when the DVB contents are 20% and 40%, the *T*-curve is approximately a straight line, which indicates the mesoporous and macroporous structures in the materials. When the DVB contents are 60% and 80%, the curve is steep at first and then becomes gentle, which indicates the presence of mesopores and micropores in the materials. By comparing the intercept of the dashed black line with the *y*-axis, it can be determined that the higher the crosslinker content, the larger the microporous volume.

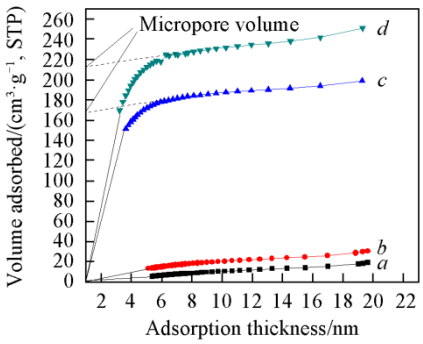

Fig.5 *T*-Plot curves of HCMPs with different concentrations of DVB at 77 K

Mass fraction of DVB(%): *a*. 20; *b*. 40; *c*. 60; *d*. 80.

All the above results indicate that the increase of DVB content can effectively produce a more uniform and narrower microporous and mesopore structure.

3.4 Magnetic Property Analysis of Magnetic-fluorescent HCMPs

In this study, *in situ* co-precipitation was used for the introduction of magnetic particles into the microporous microspheres. When the microporous microspheres and the iron salts were mixed, iron salts were attracted by the carboxyl-groups from the outer phase to bind on and inside the HCMPs. Then, with the chemical action of ammonia water and iron salts, the Fe_3O_4 nanoparticles formed. Since the formed Fe_3O_4 nanoparticles were bigger than the microsphere pore dimensions, they stayed inside the microspheres. As shown in Fig.6(A) and(B), upon exposure to an external magnetic field, the magnetic-fluorescent microspheres aggregated, leaving a clear transparent solution behind. This finding suggests that the magnetic microspheres possess strong magnetic properties. After the removal of the magnetic field, the magnetic-fluorescent microspheres can disperse uniformly in water again, which demonstrates that composite microspheres are superparamagnetic. The magnetic hysteresis loops of P(St-DVB-AA)/Fe_3O_4/CdSe/ZnS microporous microspheres measured at 50 °C are shown in Fig.7.

For the four samples(Fig.7 curves *a*—*d* represent the iron

salt concentrations of 0.5, 0.7, 1.0 and 1.5 mol/L, respectively), there are no obvious magnetic hysteresis loops observed from the field-dependent magnetization plots. All of them have similar general shapes and exhibit aero coercivity and remanence. This finding indicates they are superparamagnetic, which favors the redispersion of composite microspheres after the external magnetic field is removed. The highest saturation magnetization was found to be 38.6 A m^2/kg.

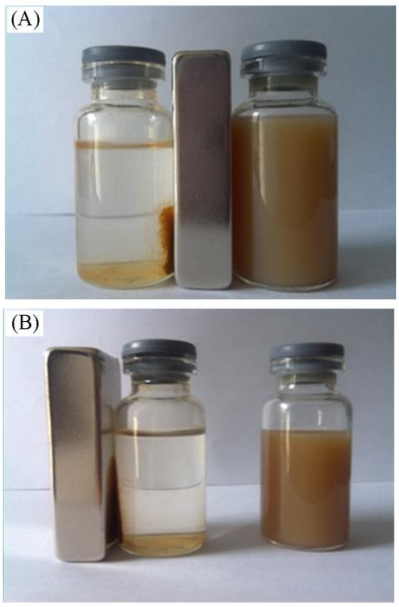

Fig.6 Optical images of magnetic fluorescent HCMPs in the presence of the external magnetic field

(A) Left: magnetic fluorescent HCMPs, right: HCMPs; (B) magnetic fluorescent HCMPs in the presence(left) and absence(right) of the external magnetic field.

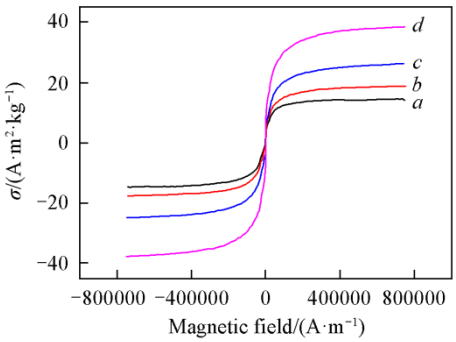

Fig.7 Magnetization curves of magnetic fluorescent HCMPs

Iron salt conentration/(mol L^{-1}): *a*. 0.5; *b*. 0.7; *c*. 1.0; *d*. 1.5.

3.5 Fluorescence Analysis of Magnetic-fluorescent HCMPs

By infusing CdSe/ZnS QDs into the swelled magnetic fluorescence microporous microspheres, with the removal of the solvent, the microspheres' structure shrank. Thus, the magnetic microspheres were incorporated with QDs successfully. Fig.8 shows the fluorescence emission spectra of magnetic fluorescence microporous microspheres. With excitation at 389 nm, the fluorescence spectrum of the magnetic-fluorescent microspheres exhibits a peak at 530 nm compared with that of the CdSe/ZnS QDs. Fig.9 shows the fluorescence micrographs of P(St/DVB/AA)/Fe_3O_4/CdSe/ZnS microporous microspheres. As shown in Fig.9(B), the composite microspheres have intense green fluorescence under the UV lamp, which has further confirmed the good incorporation of QDs within the microporous structure.

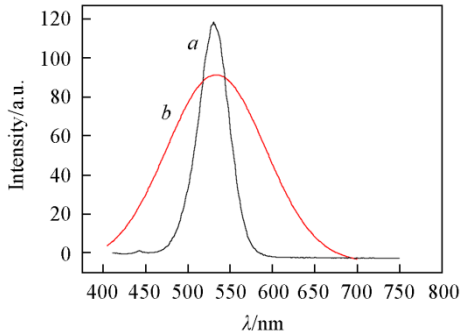

Fig.8 Fluorescence spectra of CdSe/ZnS QDs(*a*) and magnetic fluorescent HCMPs(*b*)

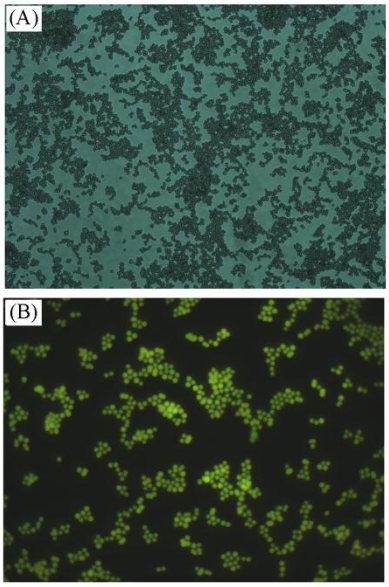

Fig.9 Fluorescent micrographs of magnetic fluorescent HCMPs under a visible light lamp(A) and an ultraviolet lamp(B)

By adding different contents of QDs in the magnetic microspheres, the fluorescence intensity of the magnetic fluorescent microspheres was analyzed. Fig.10(A)—(D) represent photographs of magnetic fluorescent microspheres when the additions of QDs are 100, 300, 500 and 700 μL, respectively. The fluorescent micrograph shows that the fluorescence intensity of microspheres increases with the increase of QDs content. In addition, Fig.10(D) shows that when the QDs content is high, the QDs exist not only in microspheres but also outside microspheres. QDs outside the microspheres have higher intensity than those in the microspheres. This finding indicates that there is an optimal content of QDs that can guarantee the QDs not to leak.

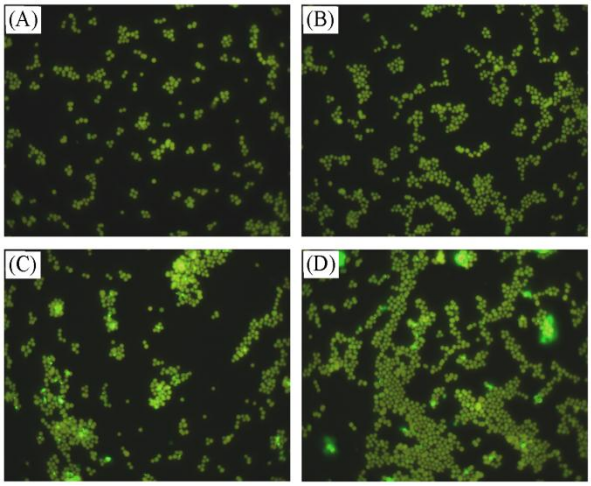

Fig.10 Effect of QDs' content on fluorescence intensity of magnetic fluorescent HCMPs

Content of QDs/μL: (A) 100; (B) 300; (C) 500; (D) 700.

4 Conclusions

In summary, using hyper-crosslinked microporous polymer microspheres(HCMPs) as templates, magnetic-fluorescent polymer microspheres were prepared successfully through *in situ* co-precipitation and swelling method with ferriferous oxide and CdSe/ZnS quantum dots as the magnetic and fluorescent sources, respectively. The BET specific surface area for the polymer was up to 703.4 m^2/g, and the pore size range was mainly between 0.7 nm and 3 nm. The high porosity enabled the loading of magnetic/fluorescent nanoparticles. VSM curves showed that the magnetic polymer microspheres are superparamagnetic, and the highest saturation magnetization was up to 38.6 A m^2/kg. The fluorescence spectrum of the magnetic-fluorescent polymer microspheres exhibited a strong green peak at 530 nm. The fluorescence microscopy images illustrate that the microspheres showed intense green fluorescence under the UV lamp, and the fluorescence intensity of microspheres increased with the increased content of QDs. The magnetic-fluorescent polymer microspheres are expected to be developed for many potential applications in diagnostic liquid biochips.

References

[1] Wu D. C., Xu F., Sun B., Fu R. W., He H. K., Matyjaszewski K., *Chem. Rev.*, **2012**, *112*, 3959

[2] Xu S. J., Liang L. Y., Li B. Y., Luo Y. L., Liu C. M., Tan B. E., *Prog. Chem.*, **2011**, *23*(10), 2085

[3] Zhang Y. B., Su J., Furukawa H., Yun Y., Gandara F., Duong A., Zou X., Yaghi O. M., *J. Am. Chem. Soc.*, **2013**, *135*(44), 16336

[4] Ding S. Y., Wang W., *Chem. Soc. Rev.*, **2013**, *42*(2), 548

[5] Rose I., Carta M., Malpassevans R., Ferrari M. C., Bernardo P., Clarizia G., Jansen J. C., McKeown N. B., *ACS Macro Lett.*, **2015**, *4*(9), 912

[6] Xie Z., Li Y. S., Chen L., Jiang D. L., *Acta Polym. Sin.*, **2016**, *12*, 1621

[7] Tan L. X., Tan B. E., *Chem. Soc. Rev.*, **2017**, 46(11), 3322

[8] Pan L., Chen Q., Zhu J. H., Yu J., He Y., Han B. H., *Polym. Chem.*, **2015**, *6*(13), 2478

[9] Hug S., Stegbauer L., Oh H., Hirscher M., Lotsch B. V., *Chem. Mater.*, **2015**, *27*(23), 8001

[10] Li W. Q., Zhang A. J., Gao H., Chen M. J., Liu A. H., Bai H., Li L., *Chem. Commun.*, **2016**, *52*(13), 2780

[11] Yang Y. W., Tan B. E., Wood C. D., *J. Mater. Chem. A*, **2016**, *4*(39), 15072

[12] Yang X., Yu M., Zhao Y., Zhang C., Wang X. Y., Jiang J. X., *J. Mater. Chem. A*, **2014**, *2*(36), 15139

[13] Islam A., Liu Z. Y., Peng R. X., Jiang W. G., Lei T., Li W., Zhang L., Yang R. J., Qian G., Ge Z. Y., *Chinese J. Polym. Sci.*, **2017**, *35*(2), 171

[14] Lin S., Diercks C. S., Zhang Y. B., Kornienko N., Nichols E. M., Zhao Y., Paris A. R., Kim D., Yang P., Yaghi O. M., Chang C. J., *Science*, **2015**, *349*(6253), 1208

[15] Das S. K., Wang X., Lai Z., *Micropor. Mesopor. Mat.*, **2017**, *255*, 76

[16] He Q., Zhang C., Li X., Wang X., Mu P., Jiang J. X., *Acta Chim. Sinica*, **2018**, *76*(3), 202

[17] Ma B. C., Ghasimi S., Landfester K., Zhang K. A. I., *J. Mater. Chem. B*, **2016**, *4*(30), 5112

[18] Huang W., Wang Z. J., Ma B. C., Ghasimi S., Gehrig D., Laquai F., Landfester K., Zhang K. A. I., *J. Mater. Chem. A*, **2016**, *4*(20), 7555

[19] Li P., Li K., Niu X., Fanet Y., *RSC Adv.*, **2016**, *6*(101), 99034

[20] Lu S., Zhang D., Liu B., Xu H., Gu H. C., *Chem. J. Chinese Universities*, **2017**, *38*(4), 509

[21] Leng Y., Wu W., Li L., Lin K., Sun K., Chen X., Li W., *Adv. Funct. Mater.*, **2016**, *26*(42), 7581

[22] Gui R. J., Wang Y. F., Sun J., *Colloids Surface B*, **2014**, *113*(1), 1

[23] Wang H. G., Sun L., Li Y. P., Fei X. L., Sun M. D., Zhang C. Q, Li Y. X., Yang Q. B., *Langmuir*, **2011**, *27*(18), 11609

[24] Yi D. K., Selvan S. T., Lee S. S., Papaefthymiou G. C., Kundaliya D., Ying J. Y., *J. Am. Chem. Soc.*, **2005**, *127*(14), 4990

[25] Guo J., Yang W., Wang C. C., He J., Chen J., *Chem. Mater.*, **2006**, *18*(23), 5554

[26] Li P., Song Y., Liu C., Li X., Zhou G., Fan Y., *Mater. Lett.*, **2014**, *114*, 132

[27] Xie M., Hu J., Wen C. Y., Zhang Z. L., Xie H. Y., Pang D. W., *Nanotechnology*, **2011**, *23*(3), 035602

[28] Tu C., Yang Y., Gao M., *Nanotechnology*, **2008**, *19*(10), 105601

[29] Weber J., Schmidt J., Thomas A., Böhlmann W., *Langmuir*, **2010**, *26*(19), 15650

[30] Galarneau A., Villemot F., Rodriguez J., Fajula F., Coasne B., *Langmuir*, **2016**, *30*(44), 13266